Elastic scattering by deterministic and random fractals: Self-affinity of the diffraction spectrum

Daniel A. Hamburger-Lidar[*]

*Racah Institute of Physics and The Fritz Haber Center for Molecular Dynamics, The Hebrew University of Jerusalem,
Jerusalem 91904, Israel*

The diffraction spectrum of coherent waves scattered from fractal supports is calculated exactly. The fractals considered are of the class generated iteratively by successive dilations and translations, and include generalizations of the Cantor set and Sierpinski carpet as special cases. Also randomized versions of these fractals are treated. The general result is that the diffraction intensities obey a strict recursion relation, and become self-affine in the limit of large iteration number, with a self-affinity exponent related directly to the fractal dimension of the scattering object. Applications include neutron scattering, x rays, optical diffraction, magnetic resonance imaging, electron diffraction, and He scattering, which all display the same universal scaling. [S1063-651X(96)11607-X]

PACS number(s): 05.40.+j, 61.43.Hv, 61.12.Bt, 02.30.Nw

I. INTRODUCTION

Scattering is one of the most important methods of observation of structural properties of matter [1–6]. Fractals, on the other hand, have in recent years received enormous attention as models for the structure of matter [7–10]. Thus the relation between the two is of very general interest, as it provides an essential connection between physical observables and the highly intriguing fractal geometry of matter. The first to consider this relation was probably Berry [11], who calculated some important averages for scattering by a random self-affine screen, coining the term ''diffractal'' for waves that have encountered fractals. In subsequent works, it was demonstrated that diffractals have properties that differ significantly from ''ordinary'' scattered waves. The central feature that distinguishes diffractals from ordinary wave fields (where geometrical optics applies) is that they are scattered by objects that have structure on all scales, in particular near their wavelength λ. This fact gives rise to various *scaling laws* of the diffraction spectrum, reflecting the fractal structure of the scattering object. In contrast, in scattering from crystalline material, characteristic interference (Bragg) *peaks* are observed, which are related through their positions to the underlying crystal structure.

In a large variety of fields scattering processes can be described by a *Fourier transform* (FT), which relates the scattering amplitude to some local density or potential. Examples (to be dealt with in some detail in Sec. II) include neutron and x-ray scattering [5], optical diffraction [1], nuclear magnetic resonance imaging (MRI) [12], electron scattering [3], and helium scattering [13]. In all these cases the FT is an approximation, but its generality and simplicity have rendered it by far the most widely used approach to scattering problems. The FT is applicable if multiple scattering and resonances can be neglected, which is typically the case under conditions of high incidence energy. A large bulk of literature, theoretical as well as experimental, exists on scattering in the FT approximation from *random* fractals.

The well-known result is that the intensity $I(q)$ decays as a power law of the momentum transfer q, with the exponent related to the fractal dimension D of the scatterer [6,14–18]. Since they are naturally less abundant, much less attention has been devoted to the scattering from fractals which can be constructed by a deterministic set of iterative rules. Scattering from such fractals, as well as randomized versions of them, will be the subject of this paper. The few examples include Berry's [11] above-mentioned work; further, mainly in optics, calculations on wave transmission [19,20] and Fraunhofer diffraction [21–24], on Cantor bars, Koch fractals, or Sierpinski-carpet like media; in x rays, numerical calculations on scattering by a Menger sponge [25], and measurements on diffraction from Cantor lattices [26]. The most extensive treatment is probably due to Allain and Cloitre [27–29]. In Ref. [28], these authors reported an optical diffraction experiment on deterministically generated Cantor bars and Vicsek fractals, and showed the resulting structure factor to be self-similar. In Refs. [27,29], they analytically solved and discussed properties such as band structure and scaling, for the diffraction problem in the case of scattering from a class of fractals similar to those to be discussed here. However, their discussion is essentially limited to Fraunhofer diffraction and does not include random fractals. Diffractal scattering for probes such as He scattering or MRI appears not to have been discussed in the literature. Thus, there seems to have been no general treatment of the diffractal-FT problem.

The purpose of the present contribution is to demonstrate that an exact solution for this problem is possible, in the case of scattering by objects on an iteratively generated *fractal support* (see Fig. 2 for an illustration of the concept). The class of fractal objects that will be considered here are those that can be generated by a combination of dilations and translations. Well-known examples of such objects include (generalizations of) the Cantor set, Vicsek fractal, and Sierpinski carpet [30]. An operator formalism will be introduced for this purpose in Sec. III, which will allow the treatment of diverse scattering conditions. It will appear in Secs. IV–VII that whereas some details of the diffraction spectrum are context sensitive (i.e., determined by a form factor), the

---

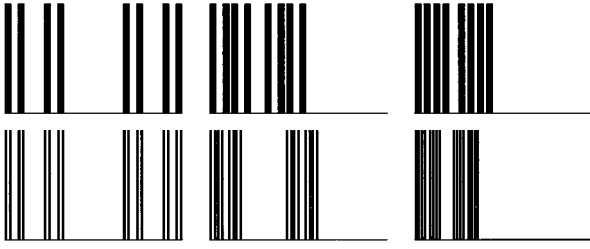*Electronic address: http://www.fh.huji.ac.il/~dani

FIG. 1. Left: third and fourth iterations of a step on a ternary Cantor set support. Middle and right: same, but with randomized translations.

overall structure is determined by a universal, context-independent scaling relation. This conclusion is unaltered (Sec. VII) by the introduction of a fractal dimension-preserving randomness. Following this finding, Secs. VIII and IX attempt to address the connection between the results derived here for a somewhat artificial class of fractals, and the standard (power-law) expressions used to interpret scattering data from natural fractals, such as self-similarity displaying porous materials, aggregates, or ramified structures.

The fractal scattering object can be generated in two essentially different ways: from bottom-up (henceforth BU—iterative inflation) or from top-down (TD—iterative refinement). In the former, the smallest unit remains fixed, and structure appears at ever larger scales, limited of course by a natural upper cutoff. This structure is reflected at ever *smaller* scales in momentum space. A fixed point is reached where further spectral details are indiscernible, either due to experimental resolution constraints or when the wavelength becomes larger than the upper cutoff. To every iteration of the fractal support there corresponds a diffraction spectrum. Subsequent diffraction-spectrum iterations may be equated when the fixed point is reached. The BU description is appropriate, e.g., in the case of a fractal formed around a single nucleation center in a deposition process, as coverage is increased. In the TD case, the total system size is fixed and structure appears at progressively smaller scales, limited by a natural lower cutoff. This description is probably more appropriate for the physical formation of fractal structures by *removal* of material (pore fractals [31]). If the wavelength λ of the incident waves is fixed, there will necessarily be another fixed point, where structure develops below λ, and further fractal details are indiscernible. Another possibility is that λ becomes smaller than the lower cutoff. In both cases subsequent iterations of the diffraction spectrum can then again be equated. Consequently, in both BU and TD cases, as will be shown here, the diffraction spectrum becomes (approximately) *self-affine*, and the self-affinity (or Hölder) exponent is simply related to the fractal dimension of the scattering object. The central result derived here is that this conclusion is unaltered neither by the physical identity of many scattering probes, nor by the introduction of a fractal dimension-preserving randomness.

II. FOURIER-TRANSFORM RELATIONS FOR COHERENT WAVE SCATTERING

The purpose of this section is to summarize the relation between the structural properties of the scattering set and the observable diffraction spectrum, for various physical examples to which the FT is applicable. The ultimate goal is to show that in spite of the apparently very different way in which the interaction (potential) between the wave and the scattering object enters the formulation in each of the cases considered, there are certain universal features in the scattering intensities, which reflect only the underlying fractal geometry of the scatterer. The different examples are presented below in increasing order of computational probe-object interaction complexity. Thus, whereas neutron scattering (Sec. II A) involves merely a discrete Fourier sum over the nuclear coordinates, electron scattering (Sec. II E) requires the FT of a potential which is a functional of the local electron density, and He scattering (Sec. II F) necessitates the Fourier transformation of a functional of the interaction potential itself. Yet, it should be emphasized that the results presented in this work, all pertain exclusively to *local* interaction potentials (as holds for all the examples considered below). Nonlocal potentials have been successfully considered in the literature as well, mainly in low-energy nuclear problems [32,33].

Notation and conventions: The momentum transfer is denoted by $\vec{q}$; the scattering amplitude by $f(\vec{q})$; spatial vectors by $\vec{r}=(x,y,z)$. Elastic scattering is assumed throughout. As emphasized in each of the subsections below, the FT is essentially always the consequence of a high-energy approximation.

A. Neutron scattering

Neutrons may couple by virtue of their spin to magnetic moments. However, the interaction of interest in the present context, i.e, which gives rise to a Fourier integral, is with nonmagnetic material, where neutrons are scattered by the nuclei. Due to the extremely short range of the strong force, this process is treated almost exactly in the Born approximation. The neutron-nucleus interaction potential [see Eq. (2.7)] is essentially a δ function (the ''Fermi pseudopotential'' [5]), so that if the nuclear positions are $\{\vec{r}_i\}$, then

$$f(\vec{q}) = C \sum_i e^{-i\vec{q} \cdot \vec{r}_i}. \tag{2.1}$$

The accuracy of this expression depends on the extent to which one may neglect incoherent scattering due to isotopes, and inelastic diffraction due to variation of the structure with time (thermal vibrations or atom diffusion).

B. X rays

The well-known Laue derivation [34] yields the relation

$$f(\vec{q}) = \int d\vec{r}\, n(\vec{r}) e^{i\vec{q} \cdot \vec{r}} \tag{2.2}$$

between the local electron concentration $n(\vec{r})$ and the x-ray scattering amplitude. The assumptions underlying the Laue derivation are essentially that the polarization and electric field intensity are linearly and locally related by the dielectric susceptibility $\chi(\vec{r})$, which itself is frequency independent. Furthermore, at the inherently *high x-ray frequencies*, $\chi \ll 1$, which allows for a decoupling of the equations result-

ing from the attempt to solve the electromagnetic wave equation in the crystal lattice, and yields Eq. (2.2).

C. Optical diffraction

The FT arises in optics in the case of Fraunhofer diffraction. This holds when both source and observation point are located very far from the aperture, although some more general conditions exist [1]. The Fraunhofer formula results from the *small-wavelength* Kirchhoff theory [35], which solves the wave equation under Huygens-Fresnel boundary conditions. The assumed smallness of the optical wavelength in comparison with the dimensions of the diffracting obstacles implies that in optical diffraction, the BU fractal construction is more natural. Essentially, Fraunhofer diffraction occurs when a coherent light wave is scattered by an object with transmission function $t(\vec{r})$, and the light amplitude is obtained by a coherent superposition

$$f(\vec{q}) = C \int d\vec{r}\, t(\vec{r}) e^{i\vec{q}\cdot\vec{r}}. \tag{2.3}$$

D. Magnetic resonance imaging

Suppose the local nuclear spin density in a sample is $\rho(\vec{r})$, and that an oscillating magnetic field with local Larmor frequency $\omega(\vec{r})$ is applied to it. It is conventionally assumed in MRI that the Larmor frequency is linear in the nuclear spin coordinates:

$$\omega(\vec{r}) = \gamma|\vec{B}_0| + \gamma\vec{G}\cdot\vec{r}, \tag{2.4}$$

where γ is the gyromagnetic ratio and $\vec{B}_0$ is the polarizing field, much larger than the linearly varying gradient field, of which $\vec{G}$ is the gradient. In practice, heterodyne mixing eliminates the term $\gamma|\vec{B}_0|$, and the integrated MRI signal amplitude can be written as

$$f(t) = \int d\vec{r}\rho(\vec{r}) e^{i\gamma\vec{G}\cdot\vec{r}t}. \tag{2.5}$$

A reciprocal space vector $\vec{q} = \gamma\vec{G}t$ is introduced [12], showing that $\vec{q}$ space may be traversed by moving either in time or in gradient magnitude, so that

$$f(\vec{q}) = \int d\vec{r}\rho(\vec{r}) e^{i\vec{q}\cdot\vec{r}}. \tag{2.6}$$

Equation (2.6) assumes *rapid signal acquisition* (after the excitation pulse), so that spin relaxation, dipolar and scalar coupling, or spin translation, do not distort the signal.

E. Scattering of electrons from atoms

Here one often applies the Born approximation,

$$f(\vec{q}) = -\frac{m}{2\pi} \int d\vec{r} e^{-i\vec{q}\cdot\vec{r}} V(\vec{r}), \tag{2.7}$$

valid at *high energies* and assuming that the electron (of mass m) sees a fixed electrostatic potential due to a charge density $n(\vec{r})$,

$$V(\vec{r}) = -e \int d\vec{r}' \frac{n(\vec{r}')}{|\vec{r}-\vec{r}'|}. \tag{2.8}$$

This expression neglects the possible polarization of the atom by the incident electron, as well as exchange effects [3].

F. He scattering

The He-surface scattering problem has been successfully treated within the sudden approximation [36,37], which assumes a *high perpendicular momentum change compared to the momentum change parallel to the surface* (essentially a high energy approximation). Under the presence of an arbitrary He-surface potential $U(\vec{R},z)$, the sudden approximation yields the scattering amplitudes as

$$f(\vec{Q}) = \frac{1}{A} \int_A d\vec{R} e^{i\vec{R}\cdot\vec{Q}} e^{2i\eta(\vec{R})}, \tag{2.9}$$

where the phase-shift function is given in the WKB approximation by

$$\eta(\vec{R}) = \int_{\xi(\vec{R})}^{\infty} dz \left[\left(k_z^2 - \frac{2m}{\hbar^2} U(\vec{R},z) \right)^{1/2} - k_z \right] - k_z\xi(\vec{R}). \tag{2.10}$$

Here $\vec{R} = (x,y)$, $\vec{Q} = (q_x,q_y)$, and k_z is the wave-number component normal to the surface. The turning points $\xi(\vec{R})$ are obtained as solutions to the energy equation

$$U[\vec{R},\xi(\vec{R})] = \frac{\hbar^2 k_z^2}{2m}, \tag{2.11}$$

with m the mass of the He atom. Effects such as resonances, multiple collisions, and dynamic polarization are neglected. For a hard-wall potential

$$U(\vec{R},z) = \begin{cases} 0, & z \geq \xi(\vec{R}) \\ \infty, & z < \xi(\vec{R}), \end{cases}$$

so that from Eq. (2.10) it follows that in this case:

$$\eta(\vec{R}) = -k_z\xi(\vec{R}), \tag{2.12}$$

as in the eikonal approximation in optics.

III. GENERATION OF FUNCTIONS ON FRACTAL SETS BY DILATION AND TRANSLATION OPERATORS

Having seen the generality of the FT in diffraction problems, the generation of the scattering fractal support is given next. The construction to be described below is in the spirit of the iterated function system formalism of Barnsley [38].
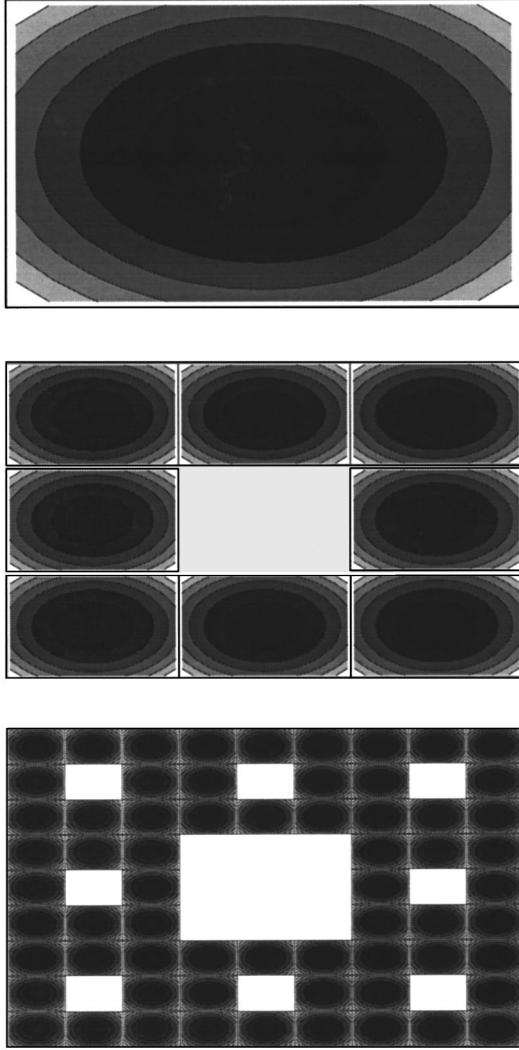
FIG. 2. Generator and first two iterations of the top-down Sierpinski carpet, supporting a harmonic potential well (contour lines). By expanding each iteration so that every square is of unit size, the corresponding bottom-up fractal can be obtained.

A. Simple example

Consider first as an introductory example the construction of a characteristic function on the usual (ternary) Cantor set (Fig. 1, left): One first contracts the generator (zero-order iteration), $\xi_0(x) = l$ $(0 < x < L)$, by a factor 3, and then places one copy of the contracted version at the origin, and another translated by $2L/3$ from the origin. This can be generalized to contractions by a factor $1/s$ $(0 < s < 1)$ and translations by aL. The corresponding TD *fractal operator* is (the reason for using the adjoint will become clear in Sec. IV)

$$\mathcal{F}^{\dagger} = (1 + \mathcal{T}_{-a})\mathcal{C}_{1/s}, \tag{3.1}$$

where the *translation operator* is defined as

$$\mathcal{T}_a h(x) = h(x + aL), \tag{3.2}$$

and the *dilation operator* is defined as

$$\mathcal{C}_s h(x) = h(sx). \tag{3.3}$$

$\mathcal{T}_a$ shifts the function it operates on by an amount aL to the left, and $\mathcal{C}_s$ stretches the function by a factor of $1/s$. When applied in the inverse sense as required by the definition of $\mathcal{F}^{\dagger}$, it is easily checked that $\xi_1(x) \equiv \mathcal{F}^{\dagger}\xi_0(x) = \xi_0(x/s) + \xi_0[(x - aL)/s]$, and that $\xi_n(x) = (\mathcal{F}^{\dagger})^n \xi_0(x)$ is indeed an nth iteration stepped Cantor surface, as illustrated in Fig. 1. Barnsley [38] and Vicsek [39] provide a general theorem for the calculation of the fractal dimension D of such iteratively constructed fractals; D is the solution of the equation

$$\sum_{i=1}^{n} s_i^D = 1, \tag{3.4}$$

where s_i are all the contraction factors. Thus in the present case:

$$\sum_{i=1}^{2} s^D = 1 \Rightarrow D = \frac{\ln(2)}{\ln(1/s)}. \tag{3.5}$$

To derive the algebraic properties of the above operators, it is convenient to express them in exponential form. $\mathcal{T}_a$ has the well-known momentum-operator representation

$$\mathcal{T}_a = e^{aL\partial_x}. \tag{3.6}$$

This can be used to find a similar representation for $\mathcal{C}_s$: Let $\mu = \ln(s)$, $y = \ln(x)$, and $g(y) = h(x)$. The argument of $h(sx)$ can then be expressed in terms of a sum: $h(sx) = h[\exp(y + \mu)] = g(y + \mu)$. But this is exactly in the form of a translation, so that using the representation of $\mathcal{T}_a$ one finds: $g(y + \mu) = \exp(\mu\partial_y)g(y)$. Noting that $\partial_y = \partial_{\ln(x)} = x\partial_x$, one obtains the desired representation:

$$\mathcal{C}_s = e^{\ln(s)x\partial_x}. \tag{3.7}$$

From here, using $\partial_x^{\dagger} = -\partial_x$ and $\partial_x x = 1 + x\partial_x$, it is easily seen that

$$\mathcal{T}_a^{\dagger} = \mathcal{T}_{-a}$$

$$\mathcal{C}_s^{\dagger} = \frac{1}{s}\mathcal{C}_{1/s}. \tag{3.8}$$

B. General construction of functions on fractals

The above formalism for TD fractals can easily be extended to arbitrary dimension, as well as to BU fractals. Let $\vec{r} = (x_1, \ldots, x_d)$ be a vector in d dimensions. Then the generalization of the one-dimensional (1D) translation and dilation operators is

$$\mathcal{T}_{\vec{a}} h(\vec{r}) = h(\vec{r} + \vec{a}L),$$

$$\mathcal{C}_s h(\vec{r}) = h(s\vec{r}). \tag{3.9}$$

In exponential representation, it is easily seen that

$$\mathcal{T}_{\vec{a}} = e^{L\vec{a}\cdot\nabla},$$

$$\mathcal{C}_s = e^{\ln(s)\vec{r}\cdot\nabla}. \tag{3.10}$$

A very wide class of fractals can be generated by using a single contraction factor s [40]:

$$\mathcal{F}^{\dagger} = \left(1 + \sum_{i=1}^{k} \mathcal{T}_{-\vec{a}_i}\right)\mathcal{C}_{1/s}. \tag{3.11}$$

For example, the Vicsek fractal [39] results by choosing

$$s = 1/3; \quad \{\vec{a}_i\} = \{(2/3,0),(1/3,1/3),(0,2/3),(2/3,2/3)\},$$

whereas the Sierpinski carpet is generated by

$$s = 1/3;$$

$$\{\vec{a}_i\} = \{(1/3,0),(2/3,0),(0,1/3),$$

$$\times(0,2/3),(1/3,2/3),(2/3,1/3),(2/3,2/3)\}$$

(Fig. 2). Equation (3.4) for the calculation of the fractal dimension applies again, and one obtains in the present case:

$$\sum_{i=1}^{k+1} s^D = 1 \Rightarrow D = \frac{\ln(k+1)}{\ln(1/s)}. \tag{3.12}$$

The BU fractal is most easily derived by employing the general fractal operator [Eq. (3.11)], and the observation that repeatedly *expanding* the TD fractal achieves the desired result. Thus the general BU fractal operator is

$$\mathcal{G}_n^{\dagger} = (\mathcal{C}_s)^n(\mathcal{F}^{\dagger})^n. \tag{3.13}$$

Note that with this definition, it is guaranteed that the smallest building block making up the fractal is of unit length. Since the expansion is one-sided, the fractal thus obtained is semi-infinite.

For future reference it is convenient to note, using Eqs. (3.8) for $\mathcal{T}_{\vec{a}}^{\dagger}$ and $\mathcal{C}_s$, that

$$\mathcal{F} = s^d \mathcal{C}_s \left(1 + \sum_{i=1}^{k} \mathcal{T}_{\vec{a}_i}\right),$$

$$\mathcal{G}_n = s^{-dn} \mathcal{F}^n \mathcal{C}_{1/s}^n. \tag{3.14}$$

IV. INTRODUCTORY EXAMPLE: ONE-DIMENSIONAL HARD-WALL He SCATTERING FROM A CANTOR SET

With the fractal operators defined, a simple but prototypical diffractal-FT problem can now be discussed. One may, e.g., consider 1D He scattering in the presence of a hard-wall potential [Eqs. (2.9) and (2.12)], with the shape function

$$\xi_n(x) = \begin{cases} l, & x \in C_n \\ 0, & \text{otherwise.} \end{cases}$$

C_n denotes the nth approximation to the Cantor set.

A. Calculation of the intensity distribution

1. TD case

Denoting the phase shift of a He atom with perpendicular wave number k_z and striking a step of height l by

$$\Phi = -2k_z l, \tag{4.1}$$

one notes that $\exp[i\Phi\xi_n(x)/l] = \exp(i\Phi)$ for $x \in C_n$ and 1 otherwise. This calls for a normalized characteristic function on the Cantor set. Such a function is just $(1/l)(\mathcal{F}^{\dagger})^n\xi_0(x)$. Therefore the scattering amplitude is [Eq. (2.9) in 1D]

$$f_n(q) = \frac{1}{L}\int_0^L dx\, e^{iqx}\frac{e^{i\Phi}}{l}[(\mathcal{F}^{\dagger})^n\xi_0(x)]$$

$$+ \frac{1}{L}\int_0^L dx\, e^{iqx}\left(1 - \frac{1}{l}[(\mathcal{F}^{\dagger})^n\xi_0(x)]\right)$$

$$= \frac{e^{i\Phi}-1}{Ll}\int_0^L dx\, [\mathcal{F}^n e^{iqx}]\xi_0(x)$$

$$+ \frac{1}{L}\int_0^L dx\, e^{iqx}\xi_0(x). \tag{4.2}$$

The last term is evidently just the specular contribution, and will henceforth be assumed subtracted out. The penultimate term contains the fractal operator, which in the present case equals [Eq. (3.14)]

$$\mathcal{F} = s\mathcal{C}_s(1 + \mathcal{T}_a). \tag{4.3}$$

What remains is to calculate $\mathcal{F}^n e^{iqx}$:

$$\mathcal{F}e^{iqx} = s\mathcal{C}_s[(1 + e^{iqaL})e^{iqx}] = s(1 + e^{iqaL})e^{iqsx},$$

$$\mathcal{F}^2 e^{iqx} = s(1 + e^{iqaL})\mathcal{F}e^{iqsx} = s^2(1 + e^{iqaL})(1 + e^{iqsaL})e^{iqs^2x}, \tag{4.4}$$

from which the general pattern can be inferred:

$$\mathcal{F}^n e^{iqx} = s^n e^{iqs^n x}\prod_{j=1}^{n}(1 + e^{iqaLs^{j-1}}). \tag{4.5}$$

This prototypical expression, or slight variants of it, will appear repeatedly when more complicated cases are treated in later sections. Before the intensities are obtained, the question of normalization must be addressed. Since the Cantor set and its generalizations discussed here have measure zero, the intensity is expected to vanish. This can be avoided if the *intensity* is normalized to the relative length occupied by the Cantor set support at the nth iteration. There are 2^n steps in the set, each of length $s^n L$, resulting in a normalization factor of $(2s)^n$.

The integration leading to the scattering amplitude [Eq. (4.2)] can now be performed, yielding, after normalization:

$$f_n(q) = \frac{1}{(2s)^{n/2}}\frac{e^{i\Phi}-1}{iqL}(e^{iqs^n L}-1)\prod_{j=0}^{n-1}(1 + e^{iqaLs^j}). \tag{4.6}$$

The last result bears some resemblance to the (complex-) Weierstrass-Mandelbrot function [7],

$$W(q) = (1-w^2)^{-1/2}\sum_{j=-\infty}^{\infty} w^j(e^{2\pi i s^j q}-1), \tag{4.7}$$

which suggests that the off-specular amplitude, as well as the intensity,

$$I_n(q) = |f_n(q)|^2, \qquad (4.8)$$

may be *self-affine* functions. Before this is investigated, consider first the BU construction.

2. BU case

Essentially, all that needs to be done is to replace the TD operator $\mathcal{F}^n$ in the preceding section everywhere by the BU operator $\mathcal{G}_n$. From Eq. (3.14) this operator is in the 1D case:

$$\mathcal{G}_n = s^{-n} \mathcal{F}^n \mathcal{C}^n_{1/s}. \qquad (4.9)$$

When this is applied to the Fourier basis set one finds

$$\mathcal{G}_n e^{iqx} = s^{-n} \mathcal{F}^n e^{is^{-n}qx} = \left[\prod_{j=1}^{n} (1 + e^{is^{j-n-1}qaL}) \right] e^{iqx}, \qquad (4.10)$$

where the last equality follows from the general result for $\mathcal{F}^n e^{iqx}$ [Eq. (4.5)]. As for normalization, since the fractal grows indefinitely in the BU case, it is most convenient to normalize the intensity by the number of elementary units. This is 2^n for the nth iteration.

In anticipation of the more general treatment of Sec. VI, the scattering amplitude $f_n(q) = (1/L)\int_0^L dx \, \exp(iqx)\exp[-2ik_z\xi_n(x)]$ can now be written as

$$f_n(q) = \left[\frac{1}{2^{n/2}} \prod_{j=0}^{n-1} (1 + e^{is^{j-n}qaL}) \right] F(q),$$

$$F(q) = \frac{1}{L} \int_0^L dx \, e^{iqx} \phi_0(x),$$

$$\phi_0(x) \equiv e^{-2ik_z\xi_0(x)}, \qquad (4.11)$$

where $F(q)$ can be interpreted as a *form factor* and the term in square brackets as a *structure factor* $S(q)$ [41].

B. Recursion relation and self-affinity of the off-specular intensity distribution

Similarly to the fractal sets described above, self-affine functions can be constructed iteratively, for example, as deterministic models of random walks [31,39,42]. At each stage, a function of this type satisfies the recursive scaling relation

$$h_{n+1}(x) = b^{-\alpha} h_n(bx), \qquad (4.12)$$

and becomes rigorously self-affine in the limit $n \to \infty$. α is denoted the Hölder, or self-affine, exponent [42]. An analogous recursion relation will now be derived for the off-specular amplitudes and intensities $I_n(q)$ of the previous sections. In the $n \to \infty$ limit, these are therefore also self-affine functions.

1. TD case

Using the result derived previously for the scattering amplitude [Eq. (4.6)], the intensity satisfies

$$I_n(q) = \frac{1}{(2s)^n} \left(\frac{2}{qL} \right)^2 [1 - \cos(\Phi)][1 - \cos(qs^n L)]$$

$$\times \left[2^n \prod_{j=0}^{n-1} [1 + \cos(qaLs^j)] \right]. \qquad (4.13)$$

The recursion-scaling relation follows once it is recognized that the scale factor b from Eq. (4.12) is the dilation factor s in the present case:

$$I_{n+1}(q) = sI_n(sq)[1 + \cos(qaL)]. \qquad (4.14)$$

Clearly, due to the presence of the cosine factor, this is not in the form of the self-affine scaling relation of Eq. (4.12), where a *constant* factor multiplies the nth iteration. However, in the TD case, successive fractal iterations will result in successive diffraction spectra that differ at ever larger q scales. q_{max}, the largest possible q, is fixed by energy conservation, irrespective of the structure of the scattering fractal set. Therefore, when the finest fractal detail, Δx_n, becomes smaller than $2\pi/q_{max}$, it becomes physically reasonable to equate successive iterations. For these to match in the sense of Eq. (4.12), the simplest criterion is to require equality of the intensities in the vicinity of the specular, $q \to 0$ (at the price of mismatch increasing with q). Proceeding thus, Eq. (4.14) will be in the form of the self-affinity relation [Eq. (4.12)] if $\cos(qaL)$ is evaluated at $q=0$. For then one finds

$$I_{n+1}(q) \approx s^{-\alpha_1} I_n(sq), \qquad (4.15)$$

where

$$\alpha_1 = D - 1 \qquad (4.16)$$

with D the fractal dimension of the Cantor set, Eq. (3.5). Thus, the self-affinity exponent of the intensity spectrum is related to the fractal dimension of the object scattered from. The reason for the specific form of the expression for α_1 will become clear in Sec. VI B. The accuracy with which Eq. (4.15) produces the required scaling can be seen in Fig. 3. Plotted there are the intensities for He scattering from a 1D hard-wall step function arrangement on two different Cantor set supports (see caption for details). Significantly, the intensities of *all maxima* (not just the specular, corresponding to $q=0$) are accurately reproduced. This situation can only be expected to improve as n is increased, demonstrating the self-affinity of the spectrum.

2. BU case

The scaling relation in this case is somewhat different from the TD fractal. From the scattering amplitude calculated for the BU fractals [Eqs. (4.11)] one finds

$$\frac{I_{n+1}(q)}{I_0(q)} = [1 + \cos(s^{-1}qaL)] \frac{I_n(q/s)}{I_0(q/s)}, \qquad (4.17)$$

implying that scaling is obeyed to within the form factor (i.e, only the structure factor, not the intensity, is fully scale invariant). For a BU fractal, features in successive diffraction spectra develop at ever *smaller* q scales. Beyond the experi-
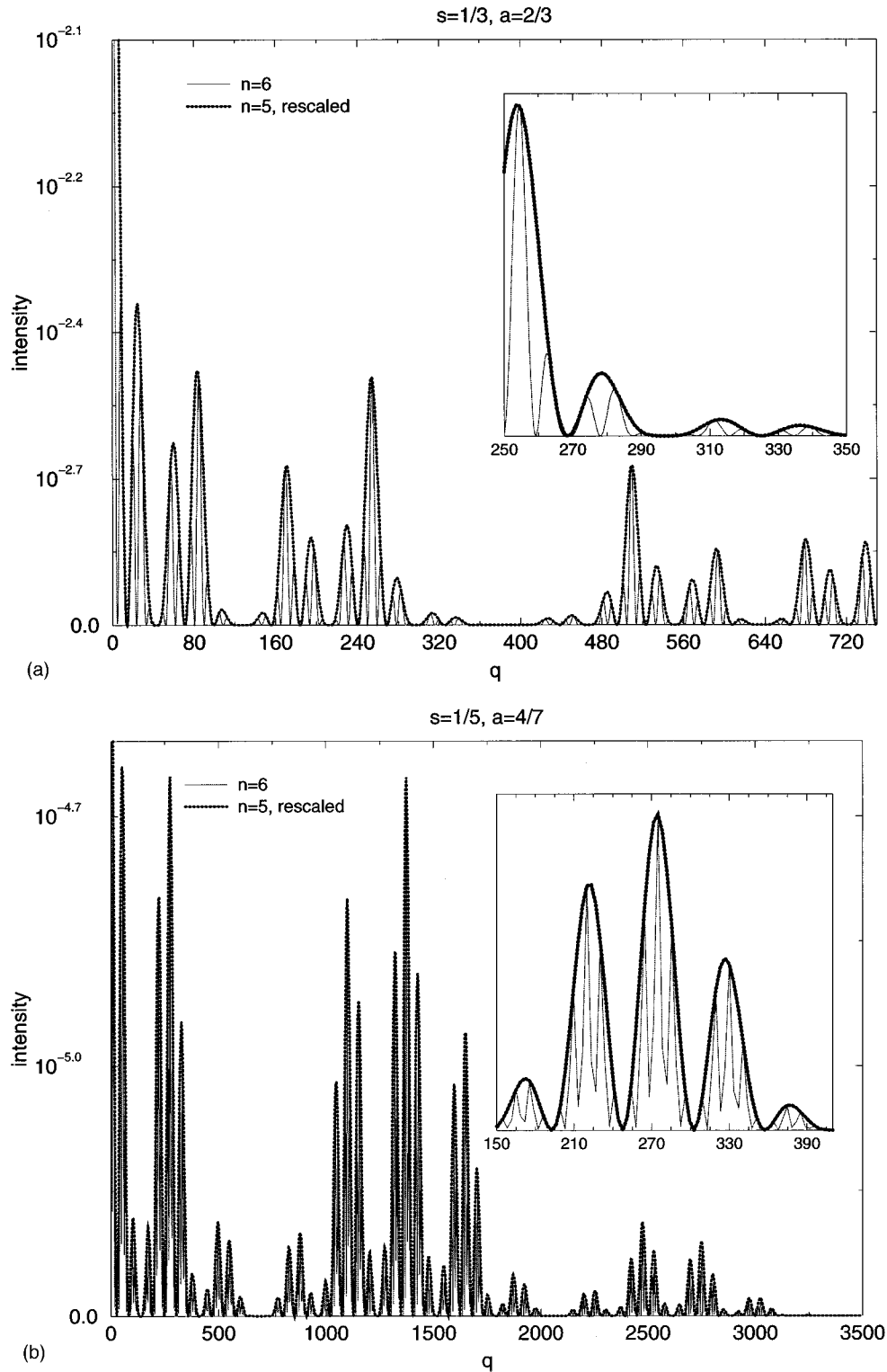
FIG. 3. Test of the scaling relation for TD fractals [Eq. (4.15)]: Superimposed intensities (arbitrary units), from Eq. (4.13), for He scattering by a hard-wall step function, built on the fifth and sixth iterations of a ternary (top) and generalized TD Cantor set with $s = 1/5$, $a = 4/7$ (bottom). The intensity from the fifth iteration (dotted line) is rescaled according to Eq. (4.15). Clearly, the rescaled intensity serves as an accurate envelope. In the $n \to \infty$ limit, therefore, subsequent iterations become indistinguishable and the intensity is self-affine. The insets show magnifications, in which a coarse-grained reproduction of the entire peak structure can be identified, illustrating the self-similarity of the spectrum.

mental q-space resolution, it is physically reasonable, as in the TD case, to compare successive iterations, and to require the intensities in the vicinity of the specular ($q \to 0$) to be equal. Substituting 1 for $\cos(qaL)$, it is now found that

where

$$\frac{I_{n+1}(q)}{I_0(q)} \approx s^{-\alpha_2} \frac{I_n(q/s)}{I_0(q/s)}, \tag{4.18}$$
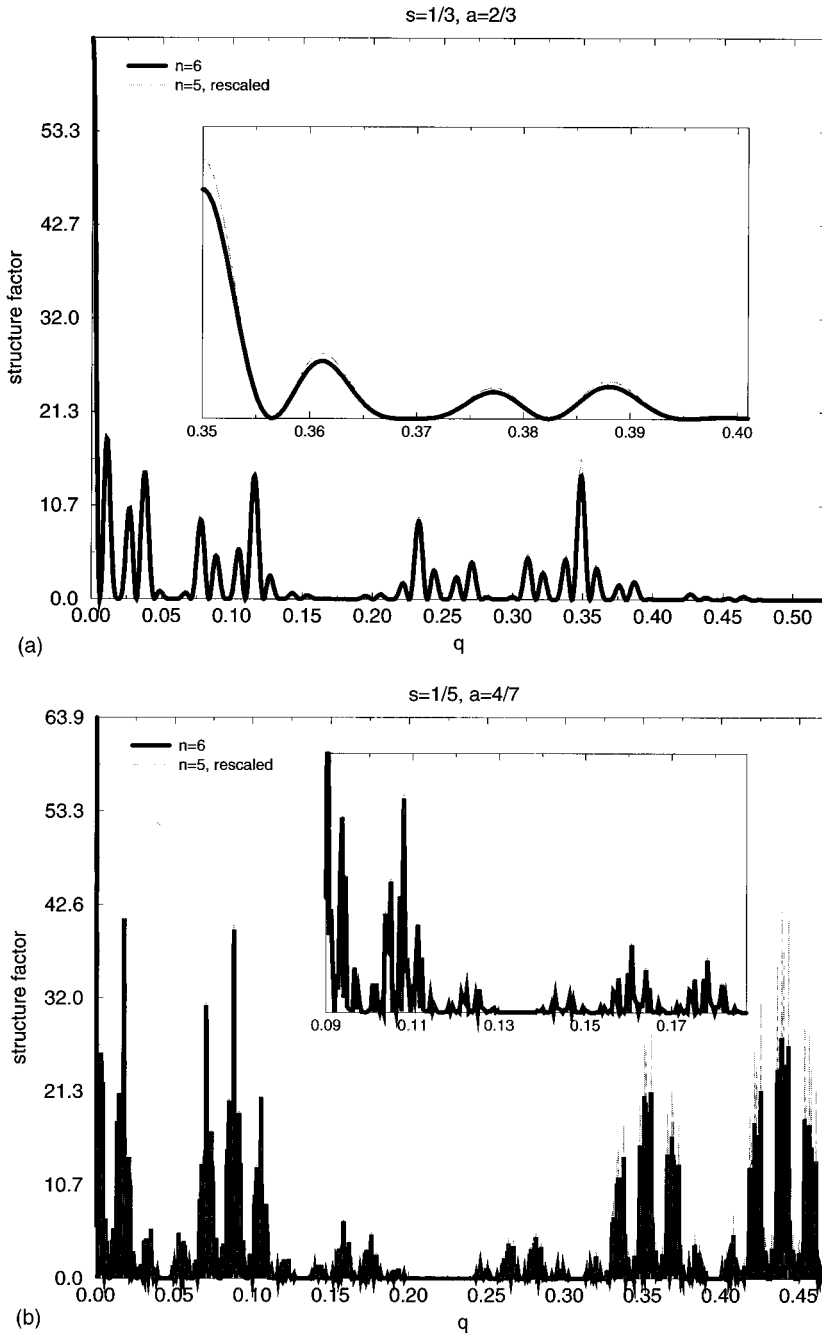
(a)

(b)

FIG. 4. *Test of the scaling relation for BU fractals [Eq. (4.18)]: Superimposed structure factors (arbitrary units), from Eq. (4.11), for He scattering by a hard-wall step function, built on the same Cantor sets as in Fig. 3. The intensity from the fifth iteration (dashed line) is rescaled according to Eq. (4.18). Again, the rescaled intensity serves as an accurate envelope, although the agreement worsens with increasing q. Insets as in Fig. 3.*

$$\alpha_2 = D, \qquad (4.19)$$

with D again the fractal dimension of the Cantor set, Eq. (3.5). This is demonstrated in Fig. 4, where the scaling recipe with α_2 is seen to hold with high accuracy.

3. Numerical check of the self-affinity

To further test the self-affinity, the Hölder exponents of the structure factors for He scattering from hard-wall step functions on an $n=8$ ternary and $n=6$, $s=1/5$, $a=4/7$ Cantor set (Fig. 4) were calculated, using the reliable and accurate *epsilon-variation* method [43,44]. The result is shown in Fig. 5. The respective regression slopes of 1.367 and 1.59, from which self-affinity exponents of $2-1.367=0.633$ and

$2-1.59=0.41$ are obtained, compare favorably with the prediction of Eq. (4.19), yielding $\alpha_2 = \ln(2)/\ln(3) = 0.631$ and $\alpha_2 = \ln(2)/\ln(5) = 0.43$. Significantly, the log-log plots are straight over two orders of magnitude, and the higher-order iteration ($n=8$) yields a more accurate exponent. Note further that this experimental-like analysis yields the same self-affinity exponent as the scaling analysis leading to Eq. (4.19), *without the $q=0$ approximation.*

In conclusion of this section, the analysis of both TD and BU fractals suggests that (1) *the scattering intensity from a fractal surface is itself (approximately) self-affine,* and (2) *the fractal dimension of the scattering surface manifests itself simply through the Hölder exponent of the scattering intensity.* Hence an analysis of the scaling properties of the scattering intensity should reveal if the scattering surface is fractal, and if so, what its fractal dimension is.
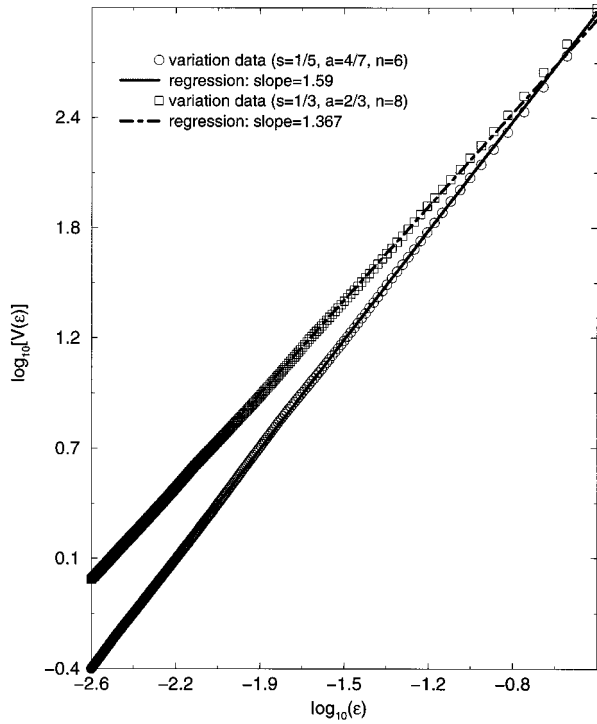
$$h_0'(x) = h_0[\phi(x)] = f\{g[\phi(x)]\} = f[g'(x)] = f[(\mathcal{P}g)(x)],$$
$$(5.4)$$

which is identical to the RHS of Eq. (5.2), so that the commutation property holds.

Note also that nothing in the above discussion restricted the result to 1D: the commutation property holds in arbitrary dimension. Thus a useful corollary follows immediately. Let $\partial G(x,z)/\partial z = g(x,z)$. Then by the commutation property:

$$\mathcal{P} \int_{\xi(x)}^{\zeta(x)} g(x,z)dz = \mathcal{P}\{G[x,\zeta(x)] - G[x,\xi(x)]\}$$

$$= G\{\phi(x),\zeta[\phi(x)]\} - G\{\phi(x),\xi[\phi(x)]\},$$

$$\int_{\mathcal{P}\xi(x)}^{\mathcal{P}\zeta(x)} \mathcal{P}g(x,z)dz = \int_{\xi[\phi(x)]}^{\zeta[\phi(x)]} g(\phi(x),z)dz$$

$$= G\{\phi(x),\zeta[\phi(x)]\} - G\{\phi(x),\xi[\phi(x)]\},$$

so that

$$\mathcal{P} \int_{\xi(x)}^{\zeta(x)} g(x,z)dz = \int_{\mathcal{P}\xi(x)}^{\mathcal{P}\zeta(x)} \mathcal{P}g(x,z)dz. \qquad (5.5)$$

FIG. 5. Results of ϵ-variation analysis [43] of the intensities displayed in Fig. 4. The slope of the log-log plots yields the self-affinity exponent as 0.633 for the $n=8$ ternary Cantor set and 0.41 for the $n=6$, $s=1/5$, $a=4/7$ set.

In the following sections it will be shown that this conclusion holds for the general (arbitrary local potential, any dimension) diffractal-FT problem. However, first a commutation property of the operators under discussion must be established. This property will make it possible to demonstrate that the scaling discussed above is indeed independent of the nature of the scattering probe, and is instead exclusively determined by the geometry of the fractal scattering object.

V. COMMUTATION PROPERTY OF CHANGE-OF-VARIABLE OPERATORS

The translation and dilation operators $\mathcal{T}_a$ and $\mathcal{C}_s$ can clearly be regarded from their definition [Eqs. (3.2) and (3.3)], as *change-of-variable operators* (COVO). Let $\mathcal{P}$ be a general COVO, i.e.,

$$\mathcal{P}p = p', \quad p'(x) = p[\phi(x)]. \qquad (5.1)$$

The purpose of this short technical section is to prove that the following commutation relation holds for COVO:

$$\mathcal{P}\{f[g(x)]\} = f[(\mathcal{P}g)(x)]. \qquad (5.2)$$

To prove this, consider the left-hand side (LHS): Let

$$f[g(x)] = h_0(x), \qquad (5.3)$$

and note that the LHS is $\mathcal{P}h_0 = h_0'$. But, by Eqs. (5.1) and (5.3),

VI. GENERAL DETERMINISTIC DIFFRACTAL−FOURIER-TRANSFORM PROBLEM

The tools are now prepared to consider the general, deterministic, diffractal-FT problem. This will require the use of the commutation property of change-of-variable operators to treat the variety of scattering probes discussed in Sec. II in a unified way.

A. Structure of the Fourier integral

The ingredients entering the general problem are (1) the FT relations from Sec. II, and (2) the realization that in every such instance, the fractal structure may be introduced into the problem by the repeated application of fractal operators to a generator $\xi_0(\vec{r})$. The structure of the general scattering amplitude is therefore

$$f_n(\vec{q}) = \int d\vec{r}\, e^{i\vec{r}\cdot\vec{q}} \phi_n(\vec{r}), \qquad (6.1)$$

where quite generally (and similarly for the TD case with $\mathcal{F}$ replacing $\mathcal{G}$),

$$\phi_n(\vec{r}) = \mathcal{A}[\mathcal{G}_n^\dagger \xi_0(\vec{r})], \qquad (6.2)$$

with $\mathcal{A}$ an operator to be specified next. For example, in the relatively simple *x-ray* case [Eq. (2.2)], $\mathcal{A}$ is the identity; $\xi_0(\vec{r}) = n_0(\vec{r})$ is the zero-order local electron density; and $\phi_n(\vec{r})$ is the electron density on the nth iteration of the fractal support. The *electron scattering* case [Eqs. (2.7) and (2.8)] is more complicated, since now $\mathcal{A}$ is an integral operator acting on $\mathcal{G}_n^\dagger(n_0(\vec{r}')/|\vec{r}-\vec{r}'|)$. But the COVO commutation property, in particular Eq. (5.5) with constant integration limits, ensures that $\mathcal{G}_n^\dagger$ can be taken out and put in front of the integral. The *He-scattering* case [Eqs. (2.9) and (2.10)] is probably the most complicated, since there the fractal op-

erator $\mathcal{G}^{\dagger}$ acts at several places simultaneously and $\mathcal{A}$ is an integral operator with a functional limit. Nevertheless, the COVO commutation property and its corollary simplify the problem to the extent that $\mathcal{G}_n^{\dagger}$ may be pulled out again:

$$f_n(\vec{Q}) = \frac{1}{A}\int_A d\vec{R}\ e^{i\vec{R}\cdot\vec{Q}}e^{2i\eta_n(\vec{R})} = \frac{1}{A}\int_A d\vec{R}(\mathcal{G}_n e^{i\vec{Q}\cdot\vec{R}})e^{2i\eta_0(\vec{R})}.$$

$$(6.3)$$

Indeed, it should now be evident that this is the general structure of the (local-potential) diffractal-FT problem: the fractal operator can always be moved from the context-specific part (ξ_0) to operate on the Fourier basis set, so that generically

$$f_n(\vec{q}) = \int d\vec{r}(\mathcal{G}_n e^{i\vec{r}\cdot\vec{q}})\phi_0(\vec{r}).$$

$$(6.4)$$

This is the general structure of the Fourier integral: a context-specific part embodied in the integrand of the form factor, $\phi_0(\vec{r})$, and *a generic part common to all diffractal-FT problems*, found in the operation of the fractal operator on the Fourier basis set. What remains, in order to understand the universal scaling behavior, is to investigate this latter part.

B. Scaling of the Fourier integral

The fractal operators to be dealt with here are of the general form given in the TD and BU cases [Eqs. (3.11) and (3.13), respectively]. The ensuing analysis closely follows along the lines of the simple 1D case treated in Sec. IV.

1. TD case

Repeating the 1D calculations of Eq. (4.4), one finds that now the application of the fractal operator yields

$$\mathcal{F}^n e^{i\vec{q}\cdot\vec{r}} = s^{nd}e^{is^n\vec{q}\cdot\vec{r}}\prod_{j=0}^{n-1}\left(1+\sum_{i=1}^{k}e^{is^j\vec{q}\cdot\vec{a}_iL}\right).$$

$$(6.5)$$

The normalization in the general case is to the relative volume occupied by the fractal, i.e., $(s^nL)^d(k+1)^n/L^d$, since there are $(k+1)^n$ fractal elements at the nth iteration, each with volume $(s^nL)^d$. Introducing a form factor,

$$F(\vec{q}) \equiv \int d\vec{r}e^{i\vec{q}\cdot\vec{r}}\phi_0(\vec{r}),$$

$$(6.6)$$

the scattering amplitude assumes the following generic form:

$$f_n(\vec{q}) = \frac{1}{[s^{nd}(k+1)^n]^{1/2}}s^{nd}\prod_{j=0}^{n-1}\left(1+\sum_{i=1}^{k}e^{is^j\vec{q}\cdot\vec{a}_iL}\right)F(\vec{q}s^n).$$

$$(6.7)$$

Thus the exact scaling relation for the intensities reads

$$I_{n+1}(\vec{q}) = \frac{s^d}{k+1}\left|1+\sum_{i=1}^{k}e^{i\vec{q}\cdot\vec{a}_iL}\right|^2 I_n(\vec{q}s),$$

$$(6.8)$$

and by employing the recipe used and justified in Sec. IV for 1D, of evaluating the exponential terms at $\vec{q}=0$, one obtains the approximate self-affinity relation

$$I_{n+1}(\vec{q}) \approx (k+1)s^d I_n(\vec{q}s).$$

$$(6.9)$$

Expressing this through the Hölder exponent as in the 1D case, $I_{n+1}(q) \approx s^{-\alpha_1}I_n(sq)$, one find that the universal relation between the self-affinity of the intensity spectrum and the fractal dimension [Eq. (3.12)], for a TD fractal support, is

$$\alpha_1 = D - d,$$

$$(6.10)$$

in agreement with the 1D case.

2. BU case

In strict analogy to the results in 1D [Eqs. (4.10) and (4.11)], one finds in the d-dimensional BU case:

$$\mathcal{G}_n e^{i\vec{q}\cdot\vec{r}} = s^{-dn}\mathcal{F}^n e^{is^{-n}\vec{q}\cdot\vec{r}}$$

$$= \left[\prod_{j=1}^{n}\left(1+\sum_{i=1}^{k}e^{is^{j-n-1}\vec{q}\cdot\vec{a}_iL}\right)\right]e^{i\vec{q}\cdot\vec{r}}, \quad (6.11)$$

$$f_n(\vec{q}) = \frac{1}{(k+1)^{n/2}}\left[\prod_{j=0}^{n-1}\left(1+\sum_{i=1}^{k}e^{is^{j-n}\vec{q}\cdot\vec{a}_iL}\right)\right]F(\vec{q}),$$

$$(6.12)$$

$$F(\vec{q}) = \int d\vec{r}\ e^{i\vec{q}\cdot\vec{r}}\phi_0(\vec{r}).$$

$$(6.13)$$

The normalization reflects that there are now $(k+1)^n$ elementary units at the nth iteration. Consequently, the scaling of the intensities is

$$\frac{I_{n+1}(\vec{q})}{I_0(\vec{q})} = \frac{1}{k+1}\left|1+\sum_{i=1}^{k}e^{is^{-1}\vec{q}\cdot\vec{a}_iL}\right|^2 \frac{I_n(\vec{q}/s)}{I_0(\vec{q}/s)}$$

$$\approx (k+1)\frac{I_n(\vec{q}/s)}{I_0(\vec{q}/s)} = s^{-\alpha_2}\frac{I_n(\vec{q}/s)}{I_0(\vec{q}/s)}, \qquad (6.14)$$

where again

$$\alpha_2 = D,$$

$$(6.15)$$

with D the fractal dimension [Eq. (3.12)] of the BU fractal support. Interestingly, it thus appears that the embedding space dimension does not enter the scaling in the BU case. This fact remains to be explained on physical grounds. To visualize the features of the intensity distribution in this case, Fig. 6 displays 1D sections of the results of He-scattering calculations from Ag adatoms centered on a sixth-generation Sierpinski carpet with an underlying Pt(111) surface (BU version of Fig. 2). These results were obtained by employing Eq. (6.12) for the structure factor, and Eq. (6.13) for the form
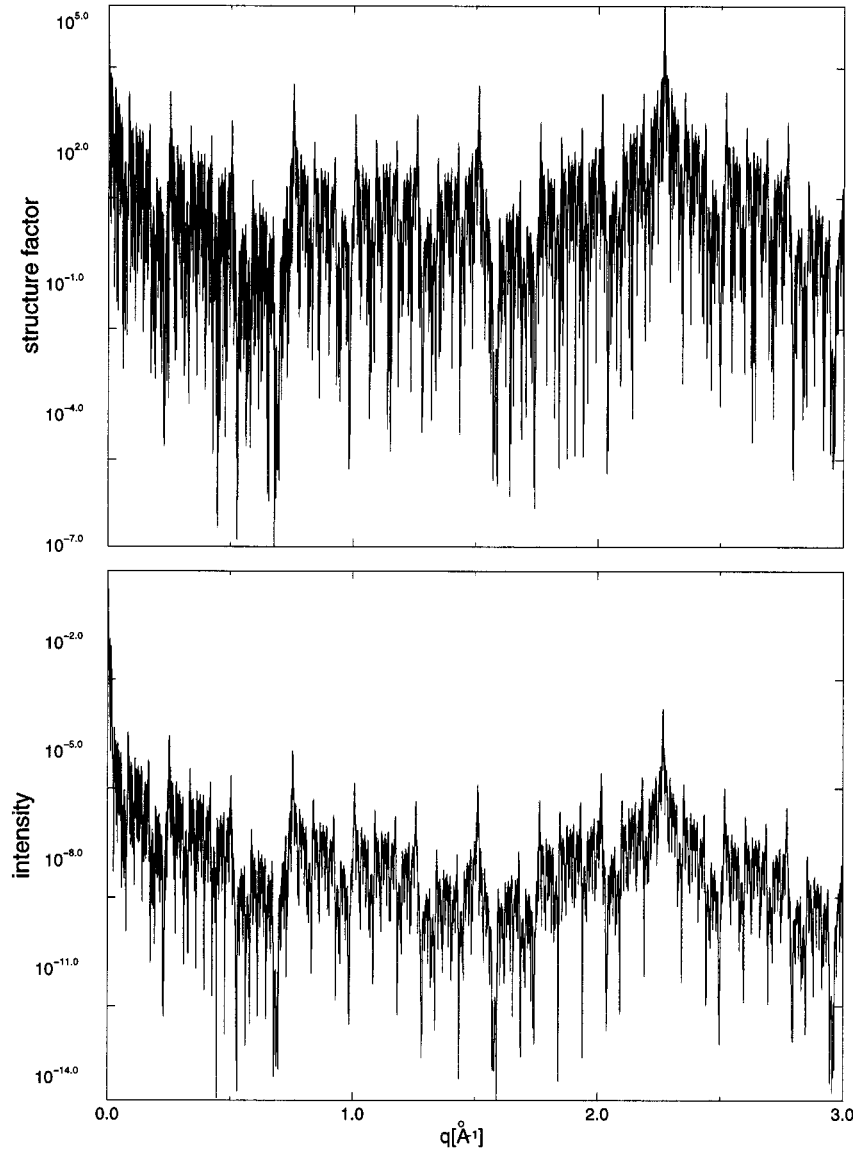
FIG. 6. Top: Structure factor for He scattering from Ag adatoms on a Pt(111) surface, with the Ag adatoms positioned on BU, sixth iteration Sierpinski carpet. The generator is a Pt(111) unit cell ($L = 2.77$Å). The self-similar structure can be noticed upon careful examination. Bottom: The complete intensity spectrum, after multiplication by the form factor (Fig. 7). The effect is mainly an overall intensity decrease with increasing q. The rainbows are too broad to be noticed as individual peaks.

factor. The latter was calculated in the sudden approximation with a realistic He-Ag-Pt potential [45] for $\phi_0(\vec{R}) = \exp[2i\eta(\vec{R})]$.

To summarize, it was shown that irrespectively of the nature of the probe, for the scattering of a coherent wave by a deterministic fractal support, the intensity spectrum is approximately self-affine, with a Hölder exponent trivially related to the fractal dimension of the support. The next generalization, necessary to approach realistic situations, concerns the effect of randomness.

VII. SCATTERING FROM A RANDOMIZED FRACTAL SUPPORT

Realistic fractals always contain some element of randomness [46]. For example, in DLA [47] the adsorbing particles perform a random walk and the resulting fractal is consequently random. Thus it is of major interest to introduce some randomness into the fractals under consideration, and to investigate its effect on the conclusions reached so far

regarding the scaling properties of the intensity distribution. In order to meaningfully introduce randomness, it is useful to *preserve the fractal dimensions of the support*. Otherwise the fractal dimension is not a useful descriptor of the scattering object. This preservation of the fractal dimension can be achieved by keeping the constant, single contraction factor, but allowing for a *distribution of translations*. The translations will be chosen independently from a given, but arbitrary, probability distribution $P(\vec{a})$, with normalization

$$\int \prod_{i=1}^{k} d\vec{a}_i^j P(\vec{a}_i^j) = 1 \qquad (7.1)$$

for each j. Here, as before, j is the iteration and i the translation-number index. The results will of course have to be averaged over the disorder ensemble, denoted by $\langle \cdots \rangle$ and defined as mean values over all possible sets $\{\vec{a}_i^j\}$. Care must be taken to apply this averaging to the observable *intensities* (and not the amplitudes), since physically, one mea-

sures the intensities from a given realization of the disorder, and averages over the different measurements. Thus

$$\langle I_n(\vec{q}) \rangle = \langle |f_n(\vec{q})|^2 \rangle = \int \prod_{j=0}^{n-1} \prod_{i=1}^{k} d\vec{a}_i^j \, P(\vec{a}_i^j) |f_n(\vec{q})|^2. \tag{7.2}$$

In order to visualize the resulting random fractal, it is useful to return momentarily to the hard-wall, stepped surface language of Sec. IV: The support with randomized translations has steps of constant width as basic building blocks, but these are spaced randomly over an underlying ''Cantor grid.'' Due to the unequal translations, however, overlaps of steps may now appear, as illustrated in Fig. 1. It will be shown next that in the present randomized case, again the intensity spectrum is self-affine, with the same relations between Hölder exponent and fractal dimensions as for the nonrandom situation.

The change from the deterministic case is that now the fractal operator is given by

$$\mathcal{F}_n^\dagger = \prod_{j=1}^{n} \left(1 + \sum_{i=1}^{k} \mathcal{T}_{-\vec{a}_i^j} \mathcal{C}_{1/s} \right), \tag{7.3}$$

where the random shifts $\{\vec{a}_i^j\}$ are chosen from $P(\vec{a})$. Since one still has two identical contractions, the fractal dimension is unchanged [Eq. (3.12)], as required.

A. TD case

Suppose a measurement is performed on a given random fractal. As for the calculations leading to the scattering amplitude in the deterministic case [Eq. (6.7)], the difference arises in that every translation $\vec{a}_i$ is replaced by $\vec{a}_i^j$, so that now

$$f_n(\vec{q}) = \frac{1}{[s^{nd}(k+1)^n]^{1/2}} s^{nd} \prod_{j=0}^{n-1} \left(1 + \sum_{i=1}^{k} e^{is^j \vec{q} \cdot \vec{a}_i^j L} \right) F(\vec{q} s^n). \tag{7.4}$$

The resulting intensities have to be averaged over the disorder ensemble:

$$\langle I_n(\vec{q}) \rangle = \frac{s^{nd}}{(k+1)^n} I_0(\vec{q} s^n) \left\langle \prod_{j=0}^{n-1} \left| 1 + \sum_{i=1}^{k} e^{is^j \vec{q} \cdot \vec{a}_i^j L} \right|^2 \right\rangle$$

$$= \frac{s^{nd}}{(k+1)^n} I_0(\vec{q} s^n) \prod_{j=0}^{n-1} \int \left[\prod_{i=1}^{k} d\vec{a}_i^j P(\vec{a}_i^j) \right]$$

$$\times \left| 1 + \sum_{i=1}^{k} e^{is^j \vec{q} \cdot \vec{a}_i^j L} \right|^2. \tag{7.5}$$

For $k=1$ (1D), since the shifts are chosen independently, the last expression simplifies into a product, and one obtains for the average intensity:

$$\langle I_n(q) \rangle = s^n I_0(q s^n) \prod_{j=0}^{n-1} [1 + \langle \cos(s^j q a_j L) \rangle] \quad \text{(1D)}. \tag{7.6}$$

In general, no such simplification occurs, but the scaling is still tractable:

$$\langle I_{n+1}(q) \rangle = \langle I_n(\vec{q} s) \rangle \frac{s^d}{k+1} \int \left[\prod_{i=1}^{k} d\vec{a}_i^0 P(\vec{a}_i^0) \right]$$

$$\times \left| 1 + \sum_{i=1}^{k} e^{i\vec{q} \cdot \vec{a}_i^0 L} \right|^2. \tag{7.7}$$

In order to express this most accurately in the approximate general self-affine form of Eq. (4.12), the average should be performed at $\vec{q}=0$. Using the normalization condition of the distribution of translations, Eq. (7.1), one finds

$$\langle I_{n+1}(q) \rangle = s^{-\alpha_1} \langle I_n(q s) \rangle, \tag{7.8}$$

with $\alpha_1 = D - d$, just as in the deterministic case [Eq. (6.10)] [48].

B. BU case

The scattering amplitude is now given by

$$f_n(\vec{q}) = \frac{1}{(k+1)^{n/2}} \prod_{j=0}^{n-1} \left(1 + \sum_{i=1}^{k} e^{is^{j-n} \vec{q} \cdot \vec{a}_i^j L} \right) F(\vec{q}). \tag{7.9}$$

Averaging the intensities over the disorder ensemble:

$$\langle I_n(\vec{q}) \rangle = \frac{1}{(k+1)^n} I_0(\vec{q}) \prod_{j=0}^{n-1} \int \left[\prod_{i=1}^{k} d\vec{a}_i^j P(\vec{a}_i^j) \right]$$

$$\times \left| 1 + \sum_{i=1}^{k} e^{is^{j-n} \vec{q} \cdot \vec{a}_i^j L} \right|^2. \tag{7.10}$$

The resulting scaling relation is

$$\frac{\langle I_{n+1}(q) \rangle}{I_0(\vec{q})} = \frac{1}{k+1} \frac{\langle I_n(\vec{q}/s) \rangle}{I_0(\vec{q}/s)} \int \left[\prod_{i=1}^{k} d\vec{a}_i^n P(\vec{a}_i^n) \right]$$

$$\times \left| 1 + \sum_{i=1}^{k} e^{is^{-1} \vec{q} \cdot \vec{a}_i^n L} \right|^2. \tag{7.11}$$

Performing the average at $q=0$, one obtains

$$\frac{\langle I_{n+1}(q) \rangle}{I_0(\vec{q})} = s^{-\alpha_2} \frac{\langle I_n(\vec{q}/s) \rangle}{I_0(\vec{q}/s)}, \tag{7.12}$$

with $\alpha_2 = D$, again as in the deterministic case [Eq. (6.15)].

To conclude, translational randomness alone appears to have no effect on the scaling properties of the diffraction spectrum.
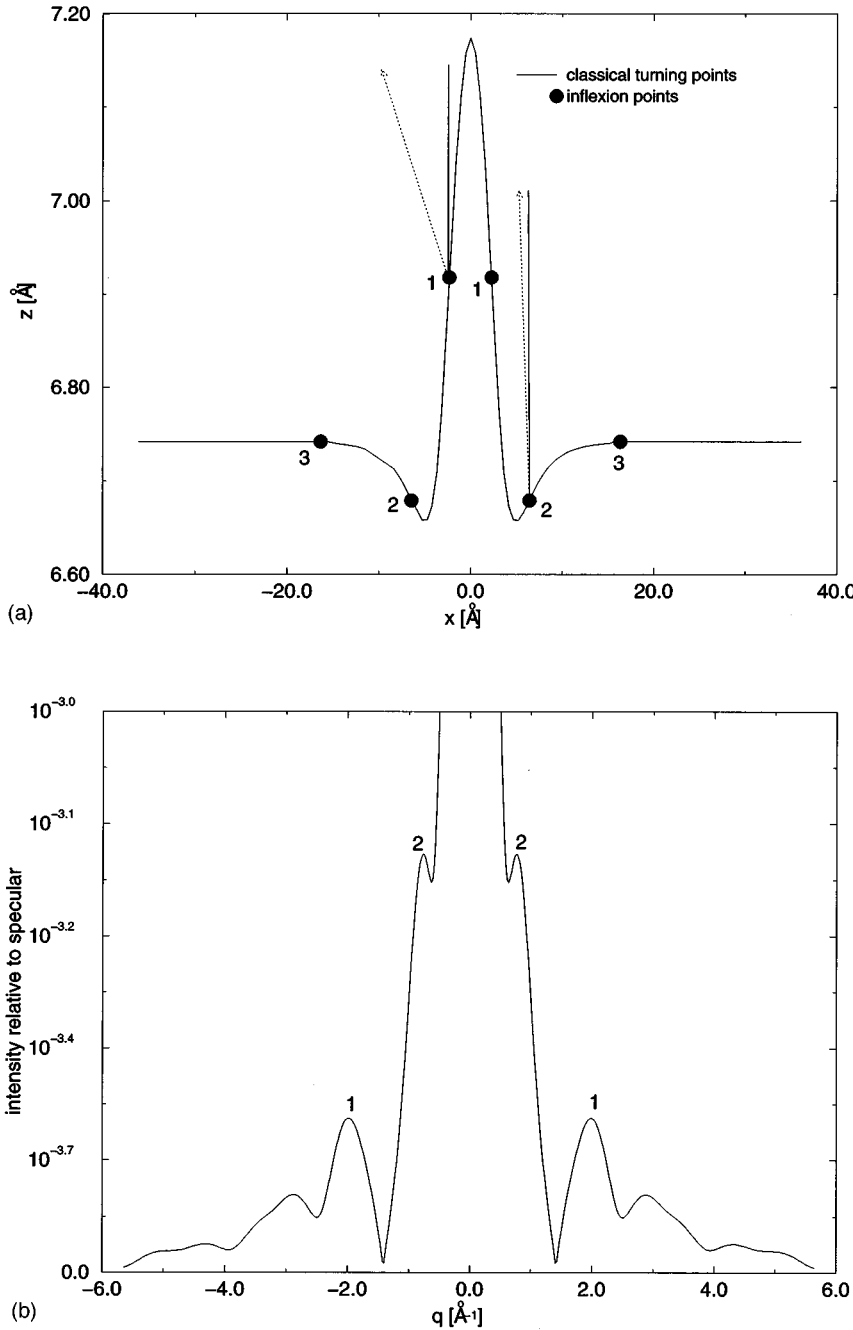
FIG. 7. Top: Classical turning points for a single Ag atom adsorbed on a flat Pt(111) surface, for He at normal incidence with $k_z = 6$ Å^{-1}. The inflexion points are indicated (1–3), along with rays (guide for the eye only), indicating the trajectories of classical particles scattered from these points (note the difference in scale between the axes, causing the apparently nonmirrorlike reflection). In the hard-wall approximation [Eq. (2.12)], the inflexion points coincide with those of the phase-shift function, and approximately yield the positions of the rainbow peaks through the stationary phase and singularity conditions [Eqs. (8.1) and (8.3)]. Using this, the scattering angles are found to be (1) 21.3° and (2) 2.4° with respect to the normal to the surface, corresponding to $q = 2.2$ and 0.25 Å^{-1}, which are approximately the rainbow positions indicated in the scattering intensity (bottom).

VIII. FURTHER PROPERTIES OF THE DIFFRACTION SPECTRUM

The diffraction spectrum is characterized by more than just its scaling properties. Such features are discussed next.

A. Role of form factor

So far, most of the discussion has centered around the universal scaling properties of the diffraction spectrum, which were completely determined by the "kinematic" structure factor. However, the role of the "dynamic" form factor cannot be ignored in discussing the properties of the spectrum. It is in this respect that the different physical probes discussed in Sec. II differ, and that universality is broken. The form factor embodies the details of the interac-

tion between probe and scatterer, and through it the potential enters the intensity spectrum. The example of He scattering will serve to illustrate the point. In this case, the He-surface interaction potential enters in a highly nontrivial way [Eq. (2.10)]. One of the striking consequences is the appearance of "rainbow" peaks in the diffraction spectrum [37]. These arise essentially whenever a He atom is scattered from an inflection point of the potential (corresponding to maximal force applied to the atom), typically due to an adsorbed cluster. Following is a brief discussion of the origin and physical significance of rainbows (see Ref. [49] for a more extensive treatment). It is useful to employ a stationary phase, approximate evaluation of the sudden approximation scattering amplitude, Eq. (2.9). In 1D, the stationary phase condition is

$$q = -2\,\eta'(x), \qquad (8.1)$$

which yields $x(q)$. The scattering amplitude is then approximated by

$$f(q) \approx \frac{e^{iq \cdot x(q)} e^{2i\eta[x(q)]}}{|\eta''|_{x(q)}}. \tag{8.2}$$

The rainbow condition is the existence of an inflection point in the phase shift:

$$\eta''(x) = 0. \tag{8.3}$$

The point x_0 satisfying this condition dominates the scattering by contributing a large peak. In the classical limit of Eq. (8.2), this shows up as a singularity in the intensity distribution, at momentum transfer q_0 satisfying the stationary phase condition [Eq. (8.1)] together with x_0. The singularity of this crude classical evaluation is smoothed into a finite peak in the more refined sudden approximation calculation.

Such sudden approximation calculations were performed for a Ag/Pt(111) BU Sierpinski-carpet system, with a realistic potential, described in detail in Ref. [45]. The results are shown in Fig. 6 (fractal system) and Fig. 7 (rainbow analysis for a single adsorbate). It appears that, although for a single adatom the rainbow peaks are a dominant feature (Fig. 7), in the case of a fractal system, their role is rather negligible in determining the structure of the spectrum (Fig. 6). The reason for this is that they are far too broad to appear as individual peaks, along with those due to the fractal support. The rainbows, as well as all other features of the form factor, act as very broad *envelopes* to the detailed spectral structure. The main effect of the form factor is to provide an overall intensity decrease, without in any way significantly altering the details of the structure factor. Since in practice one measures the full intensity distribution, this can have an effect on its self-affinity properties, and for a BU fractal care should be taken to divide by the form factor. Similar results are expected to be found in the diffraction spectra of other probes, where dynamical factors play an important role, but cannot lead to very peaked spectral features.

B. ''Bragg conditions'' and band structure

Consider the conditions for maxima derived from the scattering amplitudes for TD and BU fractals [Eqs. (6.7) and (6.12)]. For TD fractals, the condition is

$$s^j \vec{q} \cdot \vec{a}_i = \frac{2\pi t_i}{L}, \tag{8.4}$$

whereas for BU, it is

$$s^{j-n} \vec{q} \cdot \vec{a}_i = \frac{2\pi b_i}{L}. \tag{8.5}$$

Here t_i and b_i are integers, and $0 \leq j \leq n-1$. These are the ''Bragg conditions'' for iteratively generated fractals. However, since one cannot speak of a conventional unit cell with primitive lattice vectors in the fractal context, the present conditions for maxima are rather different from those for periodic crystals. For 1D Cantor-like sets, Eqs. (8.4) and (8.5) reduce to

$$s^j q = \frac{2\pi t}{La}, \quad \text{TD}, $$

$$s^{j-n} q = \frac{2\pi b}{La}, \quad BU. \tag{8.6}$$

Considering first the TD case, the maxima occur for those q's which, when multiplied by $s^0, s^1, \ldots, s^{n-1}$, are always integer multiples of $2\pi/La$. For the ternary Cantor set ($s = 1/3, a = 2/3$), with $L = 1$, these q's are all the integer multiples of $3^n \pi$. For $1/s$ equal to an arbitrary *integer*, these are the integer multiples of $(1/s)^{n-1}(2\pi/La)$. For $1/s$ noninteger, see Ref. [27]. Cast in the usual Bragg condition language, Las^{n-1} would be an effective ''lattice constant.'' The meaning of this number in the present context is similar: it is the length of the elementary building block of the fractal at the nth iteration: the union of adjacent narrow black and white bars in Fig. 1 (left). However, larger structures also repeat themselves in the fractal, with smaller frequency. These give rise to the secondary maxima in Fig. 3, and mathematically correspond to those q's which yield integer multiples of $2\pi/La$ for only a subset of $s^0, s^1, \ldots, s^{n-1}$. The incommensurability of these varying-scale repeating structures is what yields the multitude of peaks in the spectrum, as opposed to just Bragg peaks in the case of a periodic crystal, and is ultimately responsible for the self-affinity of the spectrum. The more general conditions, Eqs. (8.4) and (8.5), can be interpreted in a similar fashion.

The distinction between the BU and TD cases is straightforward: the peak spacings in the former tend to zero [with the peak nearest to the specular found at $(2\pi/La)s^n$], whereas in the latter the spacing is unbounded. The only
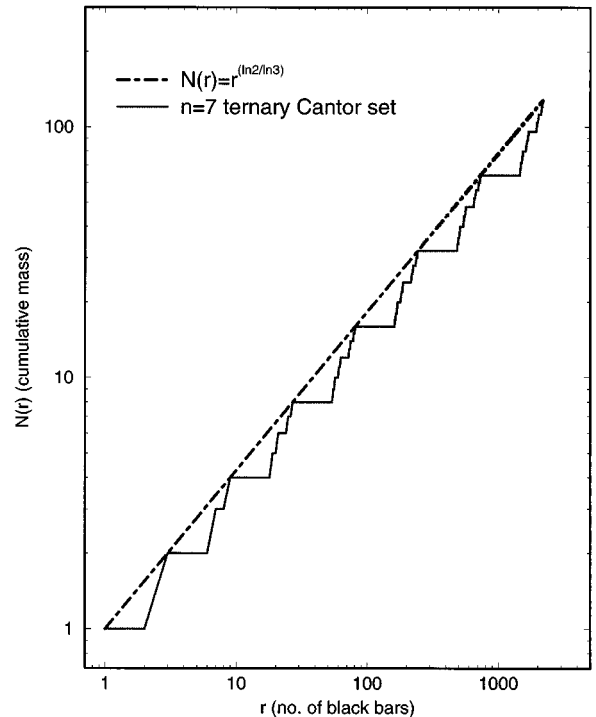

FIG. 8. Log-log plots of the exact cumulative-mass relation [Eq. (9.5)] for a seventh-iteration ternary Cantor set, and a power law with exponent equal to this set's fractal dimension [Eq. (9.1)].

limitation on the position of the furthest *observable* peak in the TD case is energy conservation. In both cases, however, the structure factors are invariant under a combination of translations and dilations (apart from the reduction in intensities, responsible for the self-affine properties). One is thus led to define a new basis of primitive vectors for the reciprocal space, from which a Brillouin zone can be constructed. As seen in Fig. 3, the regions connected by these operations do not overlap, and can be considered as separate *bands*. A detailed treatment of this point is given in Ref. [27], and will not be repeated here.

IX. SELF-AFFINE OR POWER-LAW?

As mentioned in the Introduction, the common wisdom relating to scattering by *random* fractal objects (e.g., porous solids [16,17]), amply confirmed experimentally, is that close to the specular the intensity satisfies a power law:

$$I(q) \approx q^{-\gamma}, \qquad (9.1)$$

with $\gamma = D + \text{const}$. This power-law decay is clearly very different from the self-affine intensity spectrum predicted here for iterative fractals. Considering the unquestionable experimental evidence for the power law, this discrepancy calls for clarification. The following arguments may shed some light on this issue.

In order to derive the power law [Eq. (9.1)], one typically starts with the definition of a ''mass fractal dimension,'' describing the scaling of the mass $N(r)$ enclosed in a sphere of radius r, centered at an arbitrary point in the fractal:

$$N(r) \approx r^D. \qquad (9.2)$$

If the fractal is self-averaging (an assumption which is implicit in the derivation of, e.g., Refs. [16,18]), then this mass is related to the pair distribution function $g(r)$ by

$$N(r) = \langle \rho \rangle \int_0^r g(r') d^d r', \qquad (9.3)$$

with d the embedding space dimension and $\langle \rho \rangle$ the average density. From general scattering theory it is known that the structure factor is

$$S(\vec{q}) = 1 + \langle \rho \rangle \int [g(r) - 1] e^{i\vec{q} \cdot \vec{r}} d^d r. \qquad (9.4)$$

From here one arrives at Eq. (9.1) (see Ref. [6] for details).

It is thus seen that the crucial assumption invoked in this derivation is the scaling law (9.2). It must be realized, however, that this expression is in many cases only true *on average*. This can be seen very clearly for the ternary Cantor set (Fig. 1). Suppose the set has bars of unit height and one calculates its cumulative mass $N^{(j)}$ in the jth iteration, starting from the left, and in terms of the number of black bars. Then the following recursion formula may easily be verified:

$$N^{(j+1)} = N^{(j)} \cup \{|N^{(j)}| \text{ times}[\text{ last}(N^{(j)})]\} \cup \{N_l^{(j)}$$

$$+ [\text{last}(N^{(j)})]\}_{l=1}^{|N^{(j)}|}, \quad N^{(0)} = \{1\}. \qquad (9.5)$$

Here $|N^{(j)}|$ is the length of the sequence $N^{(j)}$ and last$(N^{(j)})$ is its last term. Indeed, the zeroth-iteration ternary Cantor set consists of one black bar, the first iteration has a cumulative mass of $\{1,1,2\}$ black bars, the second iteration has mass $\{1,1,2,2,2,2,3,3,4\}$, etc. In Fig. 8 $N^{(7)}$ is displayed on a log-log plot, together with the power-law $N(r)$ (as suggested from Eq. (9.2), i.e., a line with slope ln2/ln3, the fractal dimension of the ternary Cantor set. It can be seen that this line serves as an accurate *envelope* to the actual $N(r)$, which is in fact a ''Devil's staircase,'' with a very rich (fractal) structure. This example illustrates the general situation: A simple scaling law of the form of Eq. (9.1) is only an *average* representation of the actual cumulative mass function of a fractal, which may in fact not be self-averaging. Since in this work the exact properties of the fractal [i.e., equivalent to Eq. (9.5)] were used to calculate the scattering intensities, it should now come as no surprise that the resulting diffraction spectra themselves displayed the full, rich structure of the scattering fractal object. Conversely, had the power-law form of Eq. (9.1) been used in the present scattering calculations, the result would have been a power-law decay of the intensity.

Why then do experiments from natural fractals yield the power law? The preceding arguments strongly suggest that this is related to an averaging process which smoothes the fine structure of the intensity distribution. *A priori*, two types of averages could be considered: (1) over the position of the center point of the cumulative-mass calculation, and (2) over the disorder ensemble. The first type can be ruled out immediately, however, since it is common to both the power-law and self-affine spectra derivations: The calculation of an *intensity* involves a double integral in which *all* pairs of points appear in the form $\int \int dr dr' \exp[iq(r'-r)]n(r)n(r')$. This automatically performs the first type of average. Thus, by elimination, the ensemble average appears to be responsible for smoothing out the self-affine properties into a simple power-law decay. Indeed, in the deterministic iterative fractals considered here, there is of course no ensemble to average over, in contrast to the typical experimental situation. Interestingly, the random fractals of Sec. VII are ''not random enough,'' since they also display a self-affine spectrum. The type of randomness encountered in experiments yielding the power law must lead, in contrast, to self-averaging between the physical cutoffs. There is a further difference between the randomness considered here and that encountered in experiments, namely, in the latter the randomness does not preserve the fractal dimension above the upper cutoff. In contrast, the type of randomness considered in this work preserves the fractal dimension on all scales. It is possible that this difference plays a role in creating the discrepancy between the experimental power-law results and the theory presented here.

X. CONCLUSIONS

In summary, the diffractal–Fourier-transform problem, for scattering of coherent waves from a wide class of iteratively constructed fractals, was solved analytically, yielding the scaling properties of the diffraction spectrum. The class of fractals considered here is not that which is typically observed in scattering experiments, and is characterized by a self-affine intensity spectrum. A simple relation was found to

exist between the self-affinity exponent of this spectrum and the fractal dimension of the scattering fractal support. In contrast, many experiments yield intensity distributions characterized by a power-law decay. It is argued here that this is predominantly the result of scattering from *self-averaging* random fractals, which are more abundant in experimental realizations of fractality. The results apply to a large variety of scattering probes, from neutron to He scattering, the condition being the applicability of the Fourier transform. The differences among the probes are contained in a form factor, which, however, does not seem to have an important role in determining the details of the diffraction spectrum. It would be of interest to see whether scattering from non-self-averaging (random) fractal systems will yield a self-affine

intensity spectrum as predicted here. Further theoretical work will concentrate on generalizing the types of randomness studied here, and on investigating the possible role of cutoffs in leading to the power-law decay of the intensity observed in many experiments.

[1] M. Born, *Principles of Optics*, 6th ed. (Pergamon Press, Oxford, 1980).

[2] R.G. Newton, *Scattering Theory of Waves and Particles* (McGraw-Hill, New York, 1966).

[3] J.R. Taylor, *Scattering Theory: The Quantum Theory of Non-relativistic Collisions* (Robert E. Krieger Publishing Company, Malabar, 1987).

[4] M.S. Child, *Molecular Collision Theory* (Academic Press, London, 1974).

[5] J.M. Ziman, *Models of Disorder* (Cambridge University Press, Cambridge, 1979).

[6] J. Teixeira, in *On Growth and Form*, edited by H.E. Stanley and N. Ostrowsky (Martinus Nijhoff, Boston, 1986), pp. 145–162.

[7] B. B. Mandelbrot, *The Fractal Geometry of Nature* (Freeman, San Francisco, 1982).

[8] *The Fractal Approach to Heterogeneous Chemistry: Surfaces, Colloids, Polymers*, edited by D. Avnir (John Wiley & Sons Ltd., Chichester, 1992).

[9] *Fractals in Science*, edited by A. Bunde and S. Havlin (Springer, Berlin, 1994).

[10] *On Growth and Form*, Vol. 100 of *NATO Advanced Science Institute Series E: Natural Sciences*, edited by H. E. Stanley and N. Ostrowsky (Martinus Nijhoff, Dordrecht, 1986).

[11] M.V. Berry, J. Phys. A **12**, 781 (1979).

[12] P.T. Callaghan, *Principles of Nuclear Magnetic Resonance Microscopy* (Oxford University Press, Oxford, 1991).

[13] R.B. Gerber, in *Dynamical Processes in Molecular Physics*, edited by Delgado-Bario (IOP, Bristol, 1993), p. 299.

[14] P. Pfeifer, New J. Chem. **10**, 283 (1988).

[15] J.K. Kjems, in *Fractals and Disordered Systems*, edited by A. Bunde and S. Havlin (Springer-Verlag, Berlin, 1991), pp. 263–294.

[16] H.D. Bale and P.W. Schmidt, Phys. Rev. Lett. **53**, 596 (1984).

[17] P.-z. Wong and A.J. Bray, Phys. Rev. Lett. **60**, 1344 (1988).

[18] P.-z. Wong and A.J. Bray, Phys. Rev. B **37**, 7751 (1988).

[19] V.V. Konotop, O.I. Yordanov, and I.V. Yurkevich, Europhys. Lett. **12**, 481 (1990).

[20] X. Sun and D.L. Jaggard, J. Appl. Phys. **70**, 2500 (1991).

[21] C. Iemmi and S. Ledesma, Opt. Commun. **112**, 1 (1994).

[22] D. Berger *et al.*, J. Phys. (France) I **1**, 1433 (1991).

[23] J. Guojun, F. Bihua, and F. Duan, Chem. Phys. Lett. **5**, 9 (1988).

[24] J. Uozumi, H. Kimura, and T. Asakura, J. Mod. Opt. **38**, 1335 (1991).

[25] P.W. Schmidt, J. Appl. Cryst. **24**, 414 (1991).

[26] K. Jarrendahl, M. Dulea, J. Birch and J.-E. Sundgren, Phys. Rev. B **51**, 7621 (1995).

[27] C. Allain and M. Cloitre, Phys. Rev. A **36**, 5751 (1987).

[28] C. Allain and M. Cloitre, Phys. Rev. B **33**, 3566 (1986).

[29] C. Allain and M. Cloitre, Physica A **157**, 352 (1989).

[30] It should be noted that these are *not* models of self-affine, rough surfaces, also considered in the literature [18].

[31] P. Pfeifer and M. Obert, in *The Fractal Approach to Heterogeneous Chemistry: Surfaces, Colloids, Polymers*, edited by D. Avnir (John Wiley & Sons Ltd., Chichester, 1992), pp. 38–39.

[32] K.M. Watson and J. Nutall, *Topics in Several Particle Dynamics* (Holden-Day, Inc., San Francisco, 1967).

[33] An example of a nonlocal potential is the so-called separable, or factorable, potential $V = |\zeta\rangle\langle\zeta|$, where ζ is some fixed vector in the one-particle Hilbert space. Nonlocality appears through $\langle\vec{x}'|V|\vec{x}\rangle = \zeta(\vec{x}')\zeta(\vec{x}^*)$, unlike $\delta(\vec{x}' - \vec{x})$ for the matrix element of local potentials.

[34] C. Kittel, *Introduction to Solid State Physics* (Wiley, New York, 1986).

[35] S. Silver, J. Opt. Soc. Am. **52**, 131 (1962).

[36] R.B Gerber, A.T. Yinnon, and J.N. Murrel, Chem. Phys. **31**, 1 (1978).

[37] R.B. Gerber, Chem. Rev. **87**, 29 (1987).

[38] M. Barnsley, *Fractals Everywhere* (Academic Press, Boston, 1988).

[39] T. Vicsek, *Fractal Growth Phenomena* (World Scientific, Singapore, 1989).

[40] A much richer class of dilations is possible by employing a general linear transformation, i.e., representing s by a matrix. Not all such transformations can be conveniently represented in exponential form with a single exponential, but many of them can. In particular, $\exp(x_i S_{ij}\partial_{x_j})f(x) = f(sx)$, $s = \exp(S)$. This general s is capable of providing a simultaneous rotation and stretch along arbitrarily directed axes with individual factors for each axis.

[41] A similar result was derived by Allain and Cloitre [27,28], in

the case of optical scattering in the eikonal approximation, for doubly infinite BU fractals.

[42] A.-L. Barabási and H.E. Stanley, *Fractal Concepts in Surface Growth* (Cambridge University Press, Cambridge, 1995).

[43] B. Dubuc, C. Tricot, and S.W. Zucker, Phys. Rev. A **39**, 1500 (1989).

[44] Dubuc *et al.* [43] introduced a method particularly well suited for the evaluation of the self-affinity exponent. In particular, they demonstrate that their method has the stablest *local* exponent in comparison to a variety of other methods, such as box counting and power spectrum. Briefly, in their notation, the ϵ variation of a function f is $V(\epsilon,f) = \int_0^1 v(x,\epsilon)dx$, where the ϵ oscillation $v(x,\epsilon)$ is $v(x,\epsilon) = \sup_{x' \in R_\epsilon(x)} f(x') - \inf_{x' \in R_\epsilon(x)} f(x')$, and where $R_\epsilon(x) = \{s \in [0,1]:|x-s| < \epsilon\}$. The corresponding log-log plot for the calculation of the self-affinity exponent is $[\ln(1/\epsilon), \ln[V(\epsilon,f)/\epsilon^2]]$, with the exponent given by $2-$slope.

[45] A.T. Yinnon, D.A. Hamburger, I. Farbman, R.B. Gerber, P.

Zeppenfeld, M.A. Krzyzowski and G. Comsa (unpublished).

[46] D.A. Hamburger, O. Biham, and D. Avnir, Phys. Rev. E **53**, 3342 (1996).

[47] T.A. Witten, Jr. and L.M. Sander, Phys. Rev. B **27**, 5686 (1983).

[48] It is tempting to consider also the polydisperse case, where dilations are chosen at random from a given probability distribution $P(s)$ (which is far more difficult). In this case one deals with a fractal operator of the type $\mathcal{F}_n^\dagger = \Pi_{j=1}^n (1 + \mathcal{T}_{-a}\mathcal{C}_{1/s_j})$, for which it is still possible to obtain an explicit expression for the scattering intensities, using the ideas of the preceding calculations. This will, however, not be pursued any further here, since for random dilations the fractal dimension can only be defined *on average*, and thus ceases to be a useful characteristic of the scattering set: From Eq. (3.5), $\langle D \rangle = \ln(2)\int ds\, P(s)1/\ln(1/s)$.

[49] D.A. Hamburger, A.T. Yinnon, I. Farbman, A. Ben-Shaul, and R.B. Gerber, Surf. Sci. **327**, 165 (1995).